3rd National Conference on Computational Mechanics – MekIT'05, pp. 7-22
Eds. B. Skallerud and H.I. Andersson, 11-12 May, Trondheim, Norway, 2005
Table 1 corrected (in red

HYBRID LES-RANS: Inlet Boundary Conditions

Lars Davidson

Division of Fluid Dynamics, Department of Applied Mechanics
Chalmers University of Technology, SE-412 96 Göteborg, Sweden
http://www.tfd.chalmers.se/~lada

ABSTRACT

The paper evaluates a method to prescribe synthesized turbulent inlet boundary conditions. When doing LES, DES or hybrid LES-RANS a precursor channel DNS is often used. The disadvantage of this method is that it is difficult to re-scale the DNS fluctuations to higher Reynolds numbers. In the present work synthesized isotropic turbulent fluctuations are generated at the inlet plane with a prescribed turbulent length scale and energy spectrum. A large number of independent realizations are generated. A time correlation at time step m is introduced through a linear interpolation of the running average (time step 1 to $m-1$) of the inlet profiles and realization number m. In this way an autocorrelation is prescribed.

The method is validated for hybrid LES-RANS of channel flow at $Re_\tau = 2000$ on a coarse mesh using different length and time scales of the inlet fluctuations. It is found that the time scale is more important than the length scale. Furthermore it is found that inlet time and length scales should not be equal to the correct, physical values, but should be related to the grid.

The inlet boundary conditions have much in common with forcing fluctuations at the interface in hybrid LES-RANS. In both methods the object is to *trig* the equations into describing turbulence. The method to generate inlet boundary conditions is also relevant in embedded LES, where LES is used on a mesh embedded in a global steady or unsteady RANS computation.

Keywords: inlet boundary conditions, synthesized turbulence, embedded LES, hybrid LES-RANS, LES, DES

INTRODUCTION

Inlet boundary conditions when doing Large Eddy Simulation are in many cases important. In high Reynolds number flow the grid is mostly too coarse to resolve any large portion of the turbulent spectrum. This is especially so near the inlet, where few cells commonly are located in order to reduce the number of cells; the majority of the cells are allocated to resolve boundary layers, wakes and recirculating regions. In hybrid LES-RANS and DES the grids are even coarser and the grid spacing is often larger than the turbulent integral length scale. The object of the inlet boundary conditions is then not to supply turbulence with *correct* time and length scale, but to supply scales relevant to the grid. In other words, the inlet turbulence should have integral length and time scales related to the grid size Δx, Δy, Δz and the computational time step Δt, i.e. scales that the Navier-Stokes equations on the given grid understand. The object of the inlet boundary conditions is to *trig* the equations into describing turbulence.

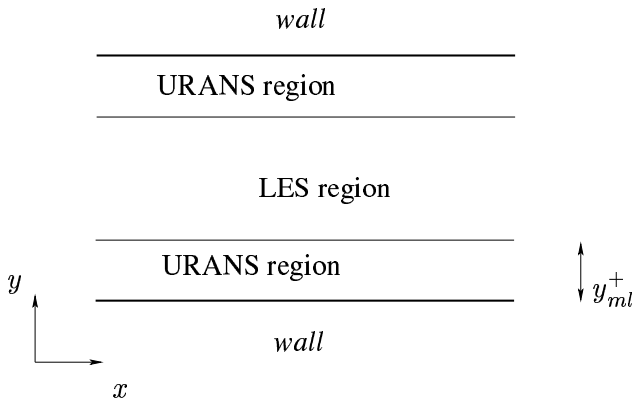

Figure 1: The LES and URANS region.

In hybrid LES-RANS, URANS (Unsteady Reynolds-Averaged Navier-Stokes) is used near the walls and at a certain distance away from the wall LES is used (Xiao et al., 2003; Davidson and Peng, 2003; Temmerman et al., 2005; Tucker and Davidson, 2004; Tucker, 2003; Hamba, 2003). The location where the switch is made from URANS to LES is called the interface. Instead of resolving the near-wall turbulent structures they are modelled with the RANS turbulence model. A drawback with hybrid LES-RANS is that at the interface where the turbulence model equations switch from URANS to LES, the LES gets poor interface conditions from the URANS. The unsteadiness which is convected from the URANS region to the LES region does not contain any proper turbulent scales. In order to supply the LES region with proper turbulent scales it was suggested to add turbulent fluctuations as momentum sources at the interface between the URANS region and the LES region. These fluctuations were either taken from a channel DNS (Davidson and Dahlström, 2004, 2005) or from synthesized turbulence (Davidson and Billson, 2004, 2005; Batten et al., 2004). The aim of these added fluctuations is – as when prescribing turbulent inlet boundary conditions – to trig the momentum equations into turbulent mode in which large-scale turbulence is resolved.

The present paper is concerned with turbulent inlet boundary conditions. Currently the most popular method to generate turbulent inlet boundary conditions is to perform a precursor DNS of channel flow or boundary layer flow. This is an accurate method provided that the Reynolds number of the DNS (based on friction velocity and boundary layer thickness) is relevant. If the Reynolds number of the DNS is too low, it is not clear how to re-scale the DNS fluctuations. While it is easy to re-scale the amplitude of the fluctuations, it is difficult to re-scale the turbulent length and time scales.

Synthesized fluctuations have previously been used in the literature by e.g. Le et al. (1997); Smirnov et al. (2001). Recently a new vortex method has been presented by Jarrin et al. (2005). One advantage of using synthesized turbulence is that the turbulent length and time scales can be prescribed independently.

Channel flow is a common test case for testing hybrid LES-RANS. Since this flow is entirely dependent on the near-wall turbulence, it is a challenging test case. It is also a useful test case for evaluating inlet boundary conditions. In the present study we are using hybrid LES-RANS, and the computational grid is – on purpose – very coarse. A mean velocity profile is prescribed, which is taken from the law of the wall. Turbulent instantaneous fluctuations are superimposed on the mean profile. These fluctuations are

taken from synthesized, isotropic turbulence prescribing the turbulent integral length scale. A large number of independent synthesized velocity field are created, which are independent of each other, which means that the time correlation is zero. By using a suitable linear combination of the running time average (from zero to time t) of the inlet fluctuations and the fluctuating field at time t the turbulent integral time scale can be prescribed. The influence of different integral length and time scales of the turbulent inlet boundary conditions is investigated.

The paper is organized as follows. First the equations and the standard hybrid LES-RANS model are presented. Next, the method to generate synthetic fluctuations is described. Then the results are presented and discussed and finally some conclusions are drawn.

EQUATIONS.

The Navier-Stokes equations with an added turbulent/SGS viscosity read

$$\frac{\partial \bar{u}_i}{\partial t} + \frac{\partial}{\partial x_j}\left(\bar{u}_i \bar{u}_j\right) = \beta \delta_{1i} - \frac{1}{\rho}\frac{\partial \bar{p}}{\partial x_i} + \frac{\partial}{\partial x_j}\left[(\nu + \nu_T)\frac{\partial \bar{u}_i}{\partial x_j}\right] \tag{1}$$

$$\frac{\partial \bar{u}_i}{\partial x_i} = 0 \tag{2}$$

where $\nu_T = \nu_t$ (ν_t denotes the turbulent RANS viscosity) for $y \leq y_{ml}$ (see Fig. 1), and for $y > y_{ml}$ we use $\nu_T = \nu_{sgs}$. The coefficient $\beta = 1$ for channel flow simulations with periodic streamwise boundary conditions; when inlet-outlet boundary conditions are used $\beta = 0$. The density is set to one in all simulations.

HYBRID LES–RANS

A one-equation model is employed in both the inner URANS region and outer LES region which reads

$$\frac{\partial k_T}{\partial t} + \frac{\partial}{\partial x_j}(\bar{u}_j k_T) = \frac{\partial}{\partial x_j}\left[(\nu + \nu_T)\frac{\partial k_T}{\partial x_j}\right] + P_{k_T} - C_\varepsilon \frac{k_T^{3/2}}{\ell} \tag{3}$$

$$P_{k_T} = -\tau_{ij}\bar{s}_{ij}, \quad \tau_{ij} = -2\nu_T \bar{s}_{ij}$$

In the inner region ($y \leq y_{ml}$) k_T corresponds to the RANS turbulent kinetic energy k; in the outer region ($y > y_{ml}$) it corresponds to the subgrid-scale kinetic turbulent energy k_{sgs}. No special treatment is used in the equations at the matching plane except that the form of the turbulent viscosity and the turbulent length scale are different in the two regions, see Table 1. At the walls $k_T = 0$ and at the inlet $\partial k_T/\partial x = 0$.

	URANS region	LES region
ℓ	$2.5n[1 - \exp(-0.2k^{1/2}n/\nu)]$	$\ell = \Delta = (\delta V)^{1/3}$
ν_T	$0.09 \cdot 2.5k^{1/2}n[1 - \exp(-0.014k^{1/2}n/\nu)]$	$0.07k_{sgs}^{1/2}\ell$
C_ε	1.0	1.07

Table 1: Turbulent viscosities and turbulent length scales in the URANS and LES regions. n and δV denote the distance to the nearest wall and the computational cell volume, respectively.

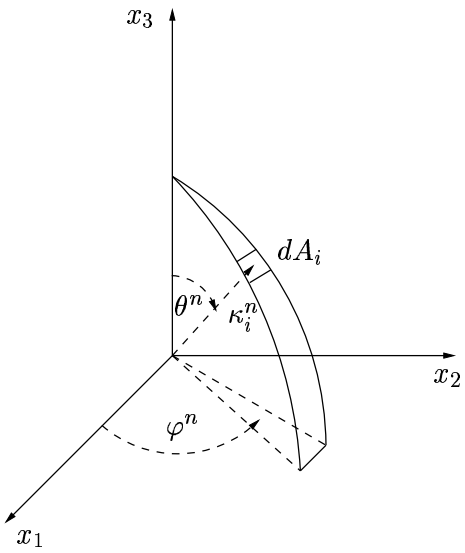

Figure 2: The probability of a randomly selected direction of a wave in wave-space is the same for all dA_i on the shell of a sphere.

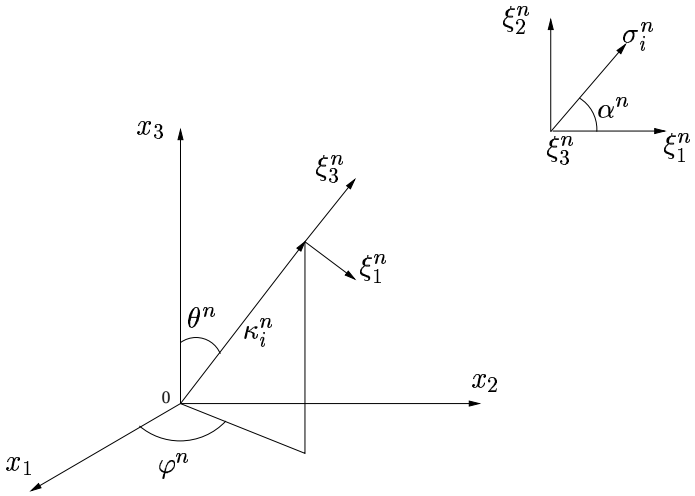

Figure 3: Definition of the unit vector σ_i^n so that $\sigma_i^n \kappa_i^n = 0$ (superscript n denotes Fourier mode n). The unit vector σ_i^n is defined so that σ_3^n is parallel to κ_i^n (i.e. $\sigma_3^n = \xi_3^n$). The direction of σ_i^n in the $\xi_1^n - \xi_2^n$ plane is randomly chosen through α.

SYNTHESIZED TURBULENCE

The fluctuations of a time-space turbulent velocity field can be simulated using N random Fourier modes as

$$u_i'(x_j) = 2 \sum_{n=1}^{N} \hat{u}^n \cos(\kappa_j^n x_j + \psi^n) \sigma_i^n \tag{4}$$

where $\hat{u}^n$, ψ^n and σ_i^n are amplitude, phase and direction of Fourier mode n. The synthesized turbulence at one time step is generated as follows. The notation follows that in Billson (2004); Billson et al. (2003); Davidson and Billson (2004, 2005) and more details can be found in these papers.

1. For each mode n, create random angles φ^n, α^n and θ^n (see Figs. 2 and 3) and random phase ψ^n.

2. Define the highest wave number based on mesh resolution $\kappa_{max} = 2\pi/(2\Delta)$ where Δ is the smallest grid spacing.

3. Define the smallest wave number from $\kappa_1 = \kappa_e/p$ where $\kappa_e = 9\pi/(55L_t)$, $L_t = Ck^{3/2}/\varepsilon$ and $C = 3$. The factor p should be larger than one to make the largest scales larger than those corresponding to κ_e. By mistake p was in the present work set to $1/3.5$ which means that the spectrum has been shifted towards larger wave numbers.

4. Divide the wavenumber space $\kappa_{max} - \kappa_1$ into N modes, equally large, of size $\Delta\kappa$.

5. Compute the randomized components of κ_j^n according to Fig. 2.

6. Continuity requires that the unit vector σ_i^n and κ_j^n are orthogonal. σ_3^n is arbitrarily chosen to be parallel with κ_i^n (see Fig. 3), and α and the requirement of orthogonality give the remaining two components.

7. A modified von Kármán spectrum is chosen. The amplitude $\hat{u}^n$ of each mode in Eq. 4 is then obtained from $\hat{u}^n = (E(|\kappa_j^n|)\Delta\kappa)^{1/2}$.

8. Having $\hat{u}^n$, κ_j^n, σ_i^n and ψ^n, the expression in Eq. 4 can be computed.

In this way inlet fluctuating velocity fields (u', v', w') are created at the inlet $y - z$ plane.

At each time step a fluctuating velocity field is generated as described above. However, they are independent of each other, and thus their time correlation will be zero. This is unphysical. To create correlation in time, new fluctuating velocity fields $\mathcal{U}'$, $\mathcal{V}'$, $\mathcal{W}'$ are computed as (Billson, 2004; Billson et al., 2003)

$$\begin{aligned}(\mathcal{U}')^m &= a(\mathcal{U}')^{m-1} + b(u')^m \\ (\mathcal{V}')^m &= a(\mathcal{V}')^{m-1} + b(v')^m \\ (\mathcal{W}')^m &= a(\mathcal{W}')^{m-1} + b(w')^m\end{aligned} \tag{5}$$

where m denotes time step number, $a = \exp(-\Delta t/\mathcal{T})$. The time correlation of $\mathcal{U}_i'$ will be equal to $\exp(-\Delta t/\mathcal{T})$, where $\mathcal{T}$ is proportional to the turbulent time scale k/ε. The inlet boundary conditions are prescribed as

$$\begin{aligned}\bar{u}(0, y, z, t) &= U_{in}(y) + u'_{in}(y, z, t) \\ \bar{v}(0, y, z, t) &= V_{in}(y) + v'_{in}(y, z, t) \\ \bar{w}(0, y, z, t) &= W_{in}(y) + w'_{in}(y, z, t)\end{aligned} \tag{6}$$

where $u'_{in} = (\mathcal{U}')^m$, $v'_{in} = (\mathcal{V}')^m$ and $w'_{in} = (\mathcal{W}')^m$ (see Eq. 5). The mean is set as $V_{in} = W_{in} = 0$ and (Welty et al., 1984)

$$U_{in}^+ = \begin{cases} y^+ & y^+ \leq 5 \\ -3.05 + 5\ln(y^+) & 5 < y^+ < 30 \\ \frac{1}{\kappa}\ln(y^+) + B & y^+ \geq 30 \end{cases} \tag{7}$$

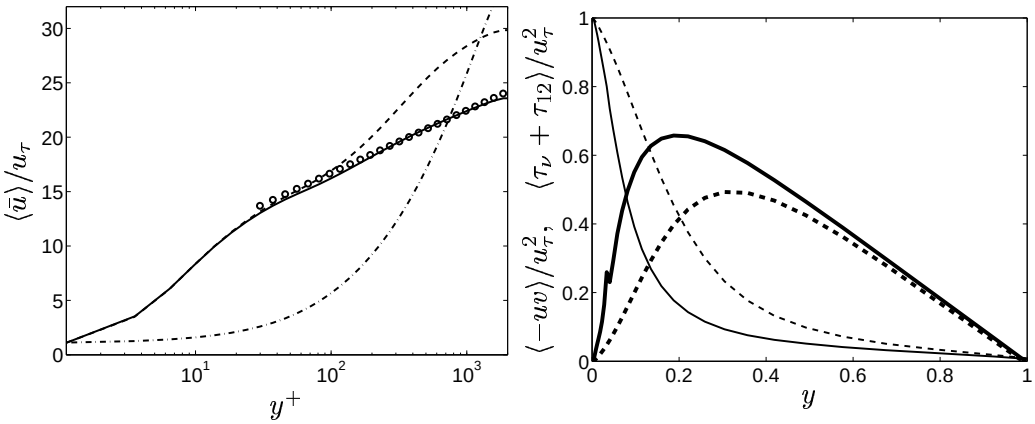

(a) $\langle \bar{u} \rangle$ profiles. ∘: $2.5 \ln(y^+) + 5.2$

(b) Shear stresses. τ_ν denotes viscous stress. Thick lines: resolved; thin lines: modelled.

Figure 4: Mean velocities and shear stresses. Periodic streamwise boundary conditions. Solid lines: forcing with isotropic fluctuations with $M_S = 0.25$; dashed lines: no forcing; dash-dotted line: LES with a one-equation k_{sgs} model.

where $\kappa = 0.4$ and $B = 5.2$

THE NUMERICAL METHOD

An incompressible, finite volume code is used (Davidson and Peng, 2003). For space discretization, central differencing is used for all terms. The Crank-Nicolson scheme is used for time discretization of all equations. The numerical procedure is based on an implicit, fractional step technique with a multigrid pressure Poisson solver (Emvin, 1997) and a non-staggered grid arrangement.

RESULTS

The mesh

The mesh has $64/32$ cells in the streamwise (x) direction for the inlet-outlet/periodic case and 32 cells in the spanwise (z) direction. The size of the computational domain is $x_{max} = 8\pi/4\pi$ (inlet-outlet/periodic case), $y_{max} = 2$ (geometric stretching of 17%) and $z_{max} = 2\pi$. This gives a Δx^+ and Δz^+ of approximately 785 and 393, respectively and $y^+ < 1$ near the walls. The location of the matching plane is at $y = 0.075$ (lower wall) which corresponds to $y^+ = 150$ and 16 cells ($= j_{ml} - 1$) in the URANS region at each wall. The time step was set to $\tau u_\tau / \delta = 4.91 \cdot 10^{-3}$. The Reynolds number is $Re_\tau = u_\tau \delta / \nu = 2000$.

Channel flow with period streamwise boundary conditions

In Fig. 4a the velocity profiles are presented using three different models: hybrid LES-RANS with and without synthesized isotropic forcing fluctuations (Davidson and Billson, 2004, 2005) and LES with a one-equation k_{sgs} model. The coefficient $M_S = 0.25$ artificially increases the streamwise turbulent length scale of the added fluctuations by a

$\mathcal{L}$	$\mathcal{T}$	$u_{\tau,22.9}/u_{\tau,in}$	a	b
$\mathcal{L}_1$	$0.25\mathcal{T}_1$	0.91	0.90	0.43
$\mathcal{L}_1$	$\mathcal{T}_1$	0.95	0.974	0.223
$\mathcal{L}_1$	$4\mathcal{T}_1$	0.97	0.994	0.113
$0.1\mathcal{L}_1$	0	0.80	0	1
$\mathcal{L}_1$	0	0.81	0	1
$0.1\mathcal{L}_1$	$\mathcal{T}_1$	0.84	0.974	0.223
$2\mathcal{L}_1$	$\mathcal{T}_1$	0.94	0.974	0.223

Table 2: Presentation of test cases. The friction velocity $u_{\tau,22.9}$ is evaluated at $x = 22.9\delta$. The turbulent length scale is set to $\mathcal{L}_1 = 0.8 = L_t$ and the turbulent time scale is set to $\mathcal{T}_1 = 0.2$ (see Section "Synthesized Turbulence"). The constants a and b from Eq. 5 are also given.

factor of four. As can be seen, the agreement with the law of the wall using hybrid LES-RANS with forcing is excellent. Without forcing, agreement is less good and using pure LES a laminar profile is obtained.

The resolved and modelled shear stresses are shown in Fig. 4b for the two hybrid models (since the resolved stress is zero for LES it is not included). The resolved stress using forcing is larger than without forcing. The reason is that the forcing fluctuations trig the resolved turbulence in the LES region. Since the total shear stress must follow $1 - y$, the modelled shear stress with forcing is smaller than without forcing.

Channel flow with inlet-outlet boundary conditions

Inlet boundary conditions are set as described in Section "Synthesized Turbulence". Neumann boundary conditions are prescribed at the outlet. In all simulations presented in this subsection, the hybrid LES-RANS without forcing has been used.

Different time and length scales of the synthesized inlet turbulent fluctuations are evaluated, see Table 2. In Fig. 5 the base-line turbulent scales $\mathcal{T}_1$ and $\mathcal{L}_1$ are used. The velocity profile (scaled with the local friction velocity $u_{\tau,x}$) is fairly well predicted and resolved turbulence is created. Further downstream the velocity in the centre region increases slightly. Reasonable levels of turbulence are generated and they increase further downstream. Note that u_{rms} is scaled with U_b since the bulk velocity is constant for all x as well as for all test cases. The circles in Fig. 5b illustrate the amplitude of the prescribed isotropic turbulence at the inlet. It is tempting to re-scale the amplitude so as to fit RMS-profiles of DNS data. However, any re-scaling with RMS profiles affects the two-point correlations of the synthetic fluctuating velocity field. Re-scaling was indeed tested, but the predicted results were worse.

When the turbulence length scale of the inlet turbulence is increased from $\mathcal{L}_1$ to $2\mathcal{L}_1$, the predicted velocity profiles and turbulence are not much affected, see Fig. 6. Next we test to take away all turbulent spacial structures by setting the turbulent length scale to $0.1\mathcal{L}_1$. This is same as setting the length scale to zero since $0.1\mathcal{L}_1 = 0.08 < \Delta z = 0.2$. Figure 7b shows that compared to Fig. 5b the turbulence generated is reduced by a factor of two close to the inlet ($x/\delta = 7.3$), but that further downstream this ratio decreases to approximately 1.6. Consequently the velocity in the centre region in Fig. 7a is much too large due to the reduced resolved shear stress.

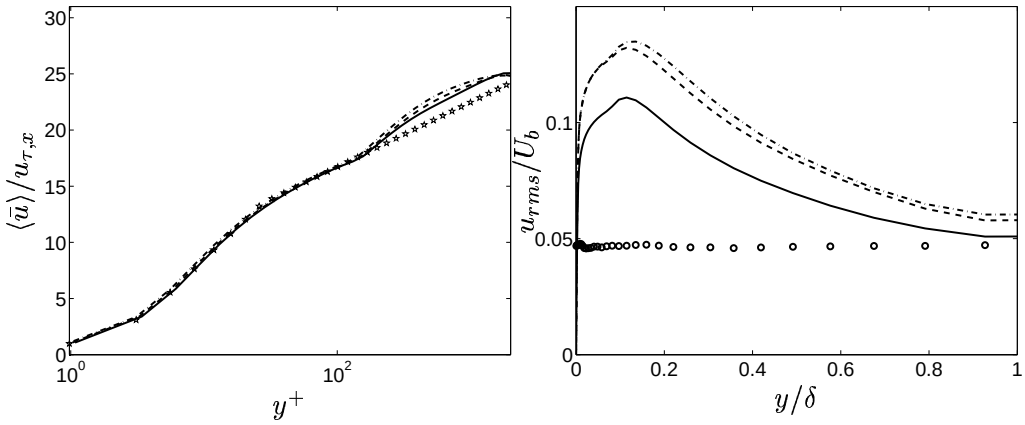

(a) $\langle\bar{u}\rangle$ profiles. ∘: $2.5\ln(y^+) + 5.2$

(b) Streamwise RMS fluctuations.

Figure 5: Mean velocities and streamwise RMS fluctuations. Inlet-outlet boundary boundary conditions. Inlet time scale $\mathcal{T}_1$ and inlet length scale $\mathcal{L}_1$. ——: $x/\delta = 7.3$; - - -: $x/\delta = 15.2$; - - -: $x/\delta = 22.9$; ∘: inlet.

In Fig. 8 the two-point correlations of the resolved turbulence at the inlet and at $x = 22.9\delta$ (both at $y^+ \simeq 60$) are presented for the inlet turbulence scales $0.1\mathcal{L}_1$, $\mathcal{L}_1$ and $2\mathcal{L}_1$. At the inlet (Fig. 8a) it can be seen that for $0.1\mathcal{L}_1$ the correlation is zero between two adjacent cells (the circles indicate the spanwise cell spacing), and the inlet fluctuations with $2\mathcal{L}_1$ have larger spanwise correlations than those with $\mathcal{L}_1$. However, far downstream (Fig. 8b), there is no difference in spanwise correlations between the $\mathcal{L}_1$ and $2\mathcal{L}_1$ cases. It can be seen that also for the case with no spanwise inlet correlation ($0.1\mathcal{L}_1$), some spanwise structures have been generated. In Fig. 8a the two-point correlation of channel DNS at $y^+ \simeq 60$ is also shown. The two-point correlation of the DNS fluctuations is actually zero at $\zeta/\delta = \Delta z$, which means that the integral turbulent spanwise length scale is smaller than the computational cell. The spanwise length scale of the inlet fluctuations is much larger than that of the DNS fluctuations, and at first, it may seem that the turbulent length scale of the inlet fluctuations should be smaller. However, as mentioned in the "Introduction", the purpose of the inlet turbulent fluctuations is to *trig* the equations into resolving turbulence. This triggering must be done at a scale which the equations understand. There is no point in using inlet turbulent fluctuations whose length scale is smaller than the grid scale. The turbulent length and time scales of the inlet fluctuations should not be as correct as possible, but they should be related to the grid scale and the time step.

Figure 9 presents velocity and u_{rms} profiles with the turbulent time scale of the inlet fluctuations set to zero ($a = 0$, $b = 1$ in Eq. 5, see Table 2). As can be seen the equations have even bigger problems to cope with zero time scale than with zero length scale. Throughout the channel the resolved streamwise stress (u_{rms}) remains smaller than the amplitude of the fluctuations prescribed at the inlet. The inlet fluctuations in Fig. 9 have structures in space with a length scale of $\mathcal{L}_1$. In Fig. 10 we impose white noise by letting also the turbulent length scale approach zero. The generated resolved fluctuations are now even smaller (compare with Fig. 9).

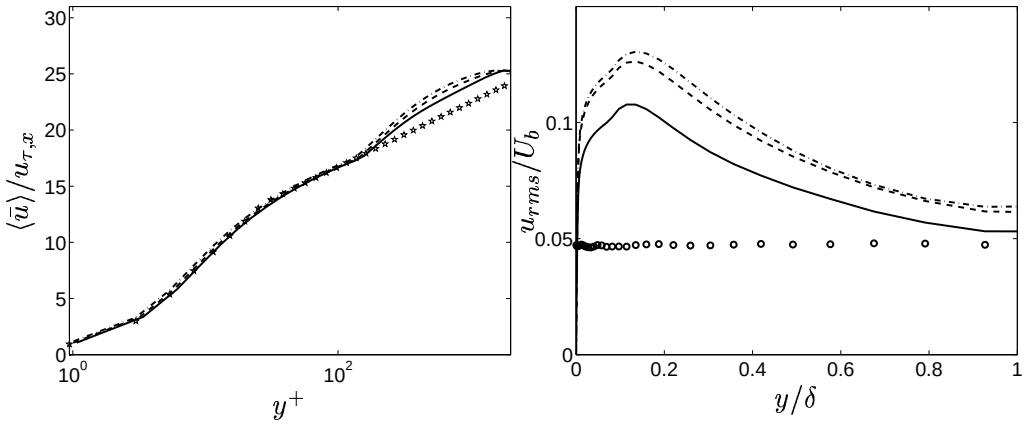

(a) $\langle\bar{u}\rangle$ profiles. ∘: $2.5\ln(y^+) + 5.2$ (b) Streamwise RMS fluctuations.

Figure 6: Mean velocities and streamwise RMS fluctuations. Inlet-outlet boundary boundary conditions. Inlet time scale $\mathcal{T}_1$ and inlet length scale $2\mathcal{L}_1$. ——: $x/\delta = 7.3$; - - -: $x/\delta = 15.2$; - · -: $x/\delta = 22.9$; ∘: inlet.

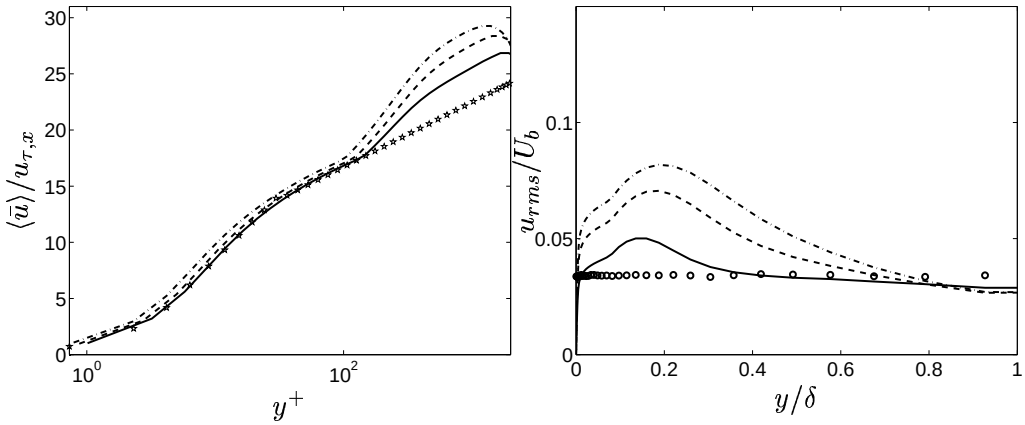

(a) $\langle\bar{u}\rangle$ profiles. ∘: $2.5\ln(y^+) + 5.2$ (b) Streamwise RMS fluctuations.

Figure 7: Mean velocities and streamwise RMS fluctuations. Inlet-outlet boundary boundary conditions. Inlet time scale $\mathcal{T}_1$ and inlet length scale $0.1\mathcal{L}_1$. ——: $x/\delta = 7.3$; - - -: $x/\delta = 15.2$; - · -: $x/\delta = 22.9$; ∘: inlet.

In Figs. 11 and 12 the influence of the time scale of the inlet turbulence is investigated. An increase of the time scale to $4\mathcal{T}_1$ improves the predicted velocity profile somewhat and increases the generated turbulence. A corresponding slight degradation of the predicted velocity profile is obtained by reducing the time scale by a factor of four, see Fig. 12.

The autocorrelations for the three cases $0.25\mathcal{T}_1$, $\mathcal{T}_1$ and $4\mathcal{T}_1$, are presented in Figs. 13-15. The autocorrelation at the inlet (solid lines) obviously increases when increasing the prescribed timescale via a and b, see Table 2. However, the autocorrelation far downstream $x = 22.9\delta$ in the URANS region (dash-dotted lines), does not increase much

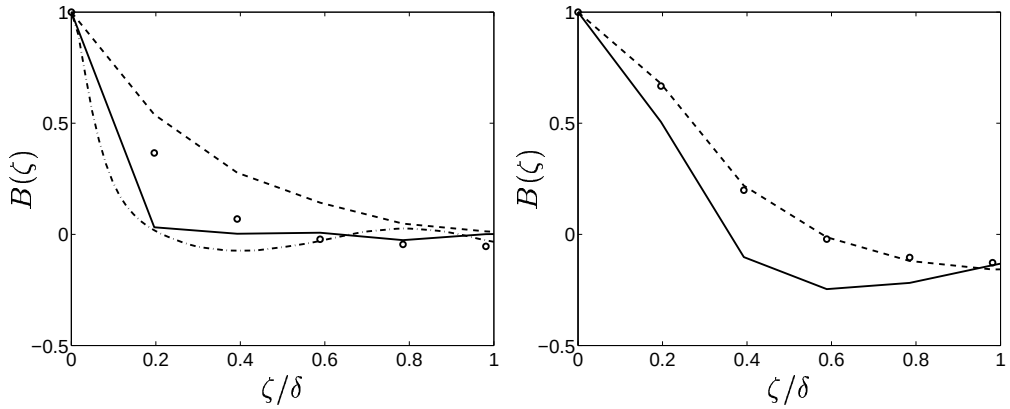

(a) $x = 0.$ - · - · : 96^3 DNS (Davidson and Billson, 2004, 2005).

(b) $x = 22.9\delta$.

Figure 8: Two point correlation $B(\zeta) = 1/(z_{max}u_{rms}^2)\int_0^{z_{max}} u'(z)u'(z-\zeta)dz$. $y^+ \simeq 60$. Time scale $\mathcal{T}_1$. ——: $0.1\mathcal{L}_1$; ∘: $\mathcal{L}_1$; - - -: $2\mathcal{L}_1$.

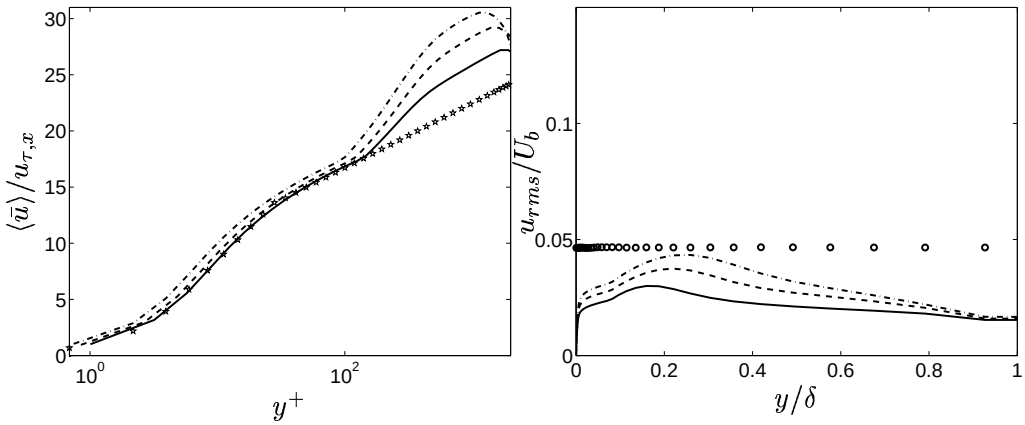

(a) $\langle\bar{u}\rangle$ profiles. ∘: $2.5\ln(y^+) + 5.2$

(b) Streamwise RMS fluctuations.

Figure 9: Mean velocities and streamwise RMS fluctuations. Inlet-outlet boundary boundary conditions. Inlet time scale $\mathcal{T} = 0$ and inlet length scale $\mathcal{L}_1$. ——: $x/\delta = 7.3$; - - -: $x/\delta = 15.2$; - - -: $x/\delta = 22.9$; ∘: inlet.

when increasing the inlet timescale from $0.25\mathcal{T}_1$ to $\mathcal{T}_1$, see Fig. 13 and 14. They both are close to $\exp(-t/\mathcal{T}_1)$. Thus the URANS equations do not respond to the short prescribed inlet time scale $0.25\mathcal{T}_1$ and the reason is probably that the short timescales are dissipated by the high turbulent RANS viscosity. In the LES region the equations respond better to the inlet time scale (dashed lines); the autocorrelations far downstream increase as the inlet timescale is increased.

Theoretically the autocorrelations of the inlet fluctuations should follow the exponential decay $\exp(-t)$. The agreement is fairly good for $\mathcal{T}_1$ in Fig. 14 but less good for $4\mathcal{T}_1$ in Fig. 15. The reason for this discrepancy is simply insufficient statistics. The co-

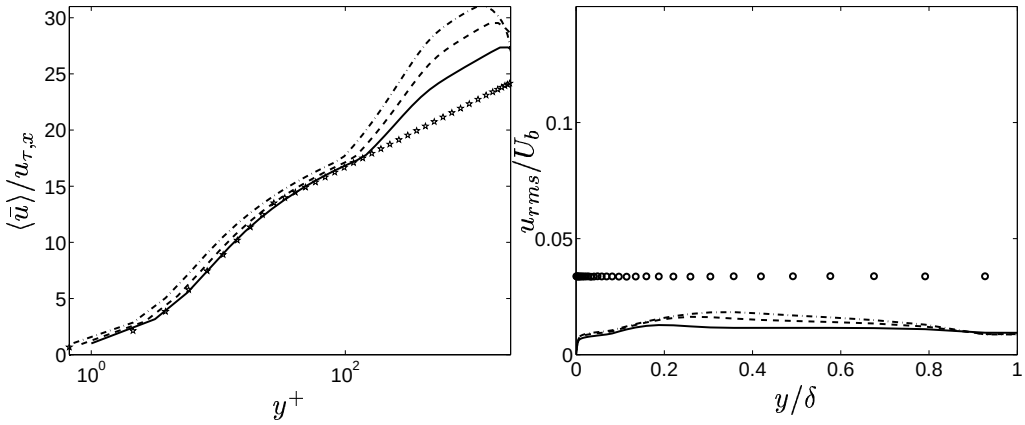

(a) $\langle\bar{u}\rangle$ profiles. ∘: $2.5\ln(y^+) + 5.2$ (b) Streamwise RMS fluctuations.

Figure 10: Mean velocities and streamwise RMS fluctuations. Inlet-outlet boundary boundary conditions. Inlet time scale $\mathcal{T} = 0$ and inlet length scale $0.1\mathcal{L}_1$. ——: $x/\delta = 7.3$; - - -: $x/\delta = 15.2$; -·-: $x/\delta = 22.9$; ∘: inlet.

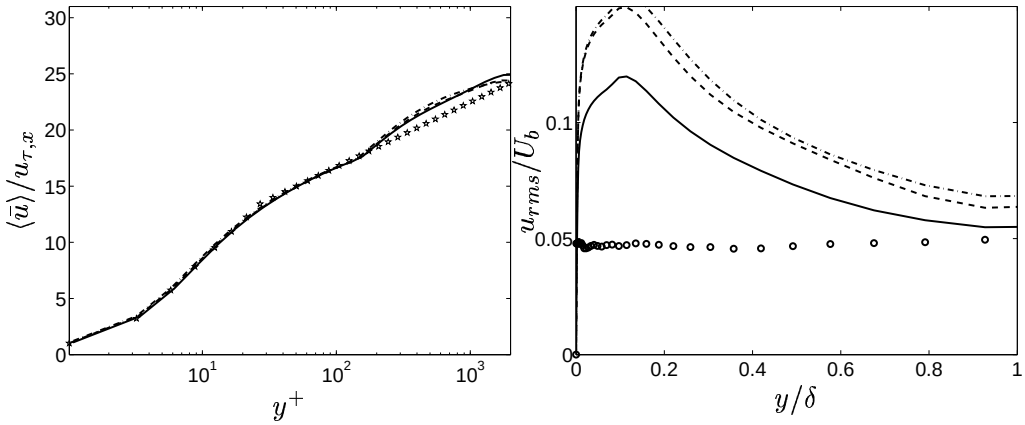

(a) $\langle\bar{u}\rangle$ profiles. ∘: $2.5\ln(y^+) + 5.2$ (b) Streamwise RMS fluctuations.

Figure 11: Mean velocities and streamwise RMS fluctuations. Inlet-outlet boundary boundary conditions. Inlet time scale $4\mathcal{T}_1$ and inlet length scale $\mathcal{L}_1$. ——: $x/\delta = 7.3$; - - -: $x/\delta = 15.2$; -·-: $x/\delta = 22.9$; ∘: inlet.

sinus function with random numbers as arguments converges very slowly. If sufficiently long time series are used the agreement should be perfect.

In Fig. 16 the predicted skin friction for all test cases are presented (numerical values of the friction velocity at $x = 22.9\delta$ are given in Table 2). As has been observed from the velocity profiles, worst results are obtained for the cases for which the time scale $\mathcal{T}$ is set to zero. It can also be seen that it is better to prescribe a timescale with zero length scale ($\mathcal{T}_1$ and $0.1\mathcal{L}_1$) than vice versa. With an inlet turbulent length scale of $\mathcal{L}_1$ the predicted skin friction gets better the larger the time scale. When the inlet length scale is increased to $2\mathcal{L}_1$ the predicted results deteriorate slightly.

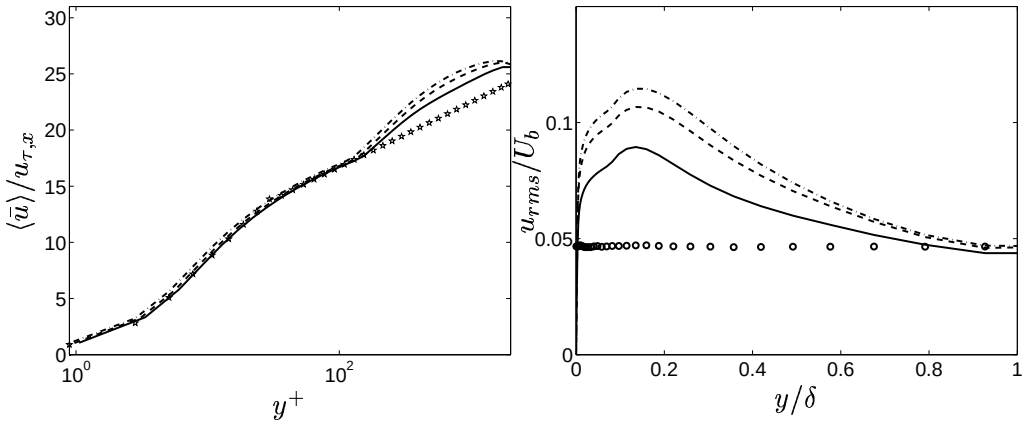

(a) $\langle\bar{u}\rangle$ profiles. ∘: $2.5\ln(y^+)+5.2$ (b) Streamwise RMS fluctuations.

Figure 12: Mean velocities and streamwise RMS fluctuations. Inlet-outlet boundary boundary conditions. Inlet time scale $0.25\mathcal{T}_1$ and inlet length scale $\mathcal{L}_1$. ——: $x/\delta = 7.3$; - - -: $x/\delta = 15.2$; - - -: $x/\delta = 22.9$; ∘: inlet.

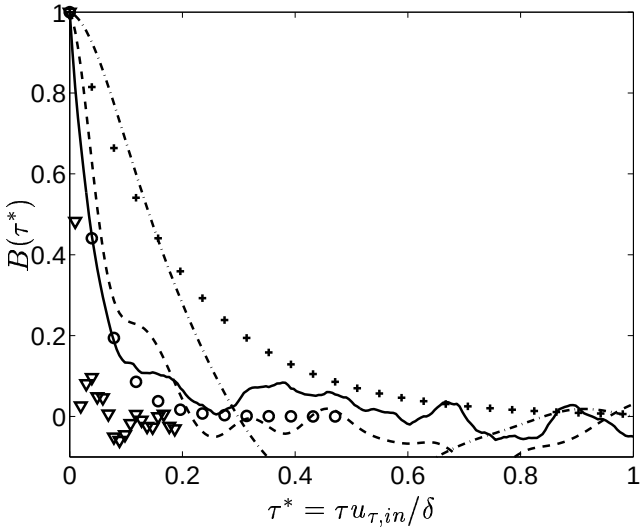

Figure 13: Autocorrelation $B(\tau) = 1/(Tu_{rms}^2)\int_0^T u'(t)u'(t-\tau)dt$. Time scale $0.25\mathcal{T}_1$ (see Eq. 5). ▽: 96^3 channel DNS (Davidson and Billson, 2005); ∘: $0.25\exp(-t)/\mathcal{T}_1$; +: $\exp(-t)/\mathcal{T}_1$; ——: inlet; - - -: $x = 22.7\delta$, $y^+ = 840$; -·-: $x = 22.7\delta$, $y^+ = 37$.

The solid line in Fig. 16 exhibits typical odd-even oscillations. This is due to the coarse mesh and central differencing. These oscillations could easily be damped out using a wiggle detector (Dahlström and Davidson, 2003), but since they are not causing any problems no damping has been used. Oscillations are present for all cases but all lines/markers except the solid line are plotted for every second x node to enhance visibility.

CONCLUSIONS

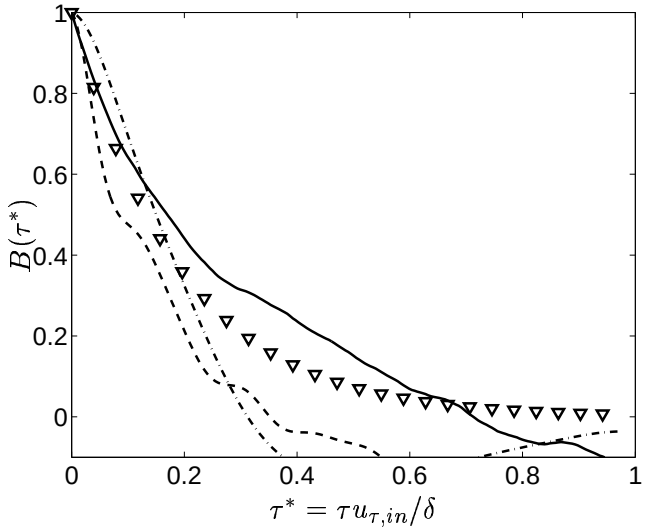

Figure 14: Autocorrelation $B(\tau)$. Time scale $\mathcal{T}_1$ (see Eq. 5). $\triangledown$: $\exp(-t)/\mathcal{T}_1$; —— : inlet; - - - : $x = 22.7\delta$, $y^+ = 840$; - - - : $x = 22.7\delta$, $y^+ = 37$.

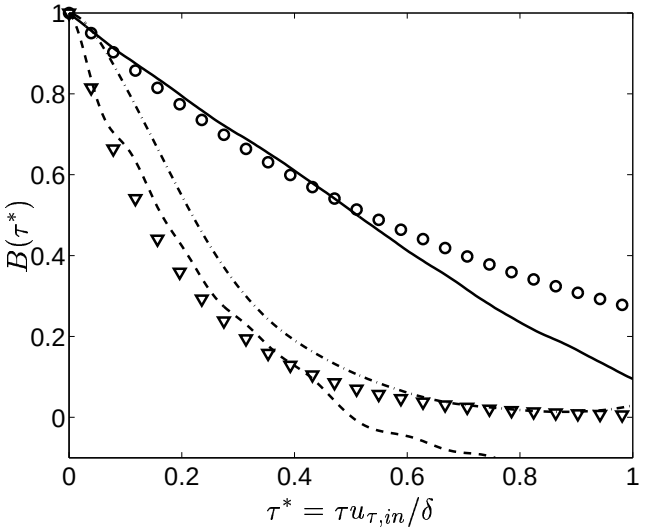

Figure 15: Autocorrelation $B(\tau)$. Time scale $4\mathcal{T}_1$ (see Eq. 5). $\circ$: $\exp(-t)/(4\mathcal{T}_1)$; $\triangledown$: $\exp(-t)/\mathcal{T}_1$; —— : inlet; - - - : $x = 22.7\delta$, $y^+ = 840$; - - - : $x = 22.7\delta$, $y^+ = 37$.

In the present paper synthetic fluctuations have been used for generating inlet turbulent fluctuating boundary conditions. The mean profile was taken from the law of the wall. It has been found that this approach is an efficient method to generate inlet boundary conditions. The role of the fluctuations is not to be as physically correct as possible, but to *trig* the equations into resolving turbulence.

By mistake the spectrum of the synthetic fluctuations used in all the simulations was shifted towards higher wave numbers. It is not clear how large an influence this shift has on the predicted results. The predictions are currently being repeated with a more correct spectrum.

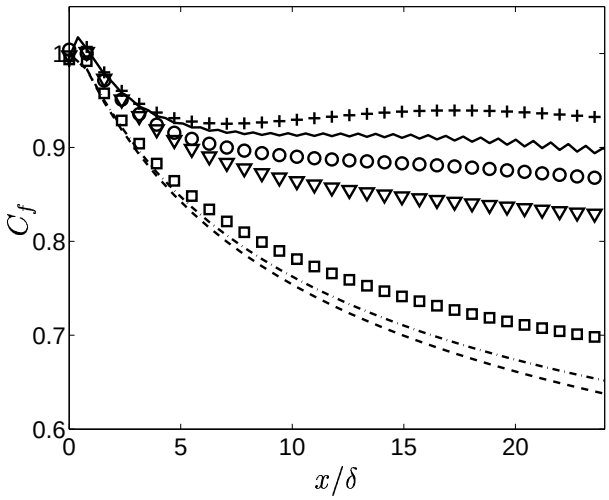

Figure 16: Skin friction. —— : $\mathcal{T}_1$ and $\mathcal{L}_1$; ○: $\mathcal{T}_1$ and $2\mathcal{L}_1$; +: $4\mathcal{T}_1$ and $\mathcal{L}_1$; ▽: $0.25\mathcal{T}_1$ and $\mathcal{L}_1$; □: $\mathcal{T}_1$ and $0.1\mathcal{L}_1$; - - - : $\mathcal{T} = 0$ and $\mathcal{L}_1$; - - - : $\mathcal{T} = 0$ and $0.1\mathcal{L}_1$.

Acknowledgments.

This work was financed by the DESider project (Detached Eddy Simulation for Industrial Aerodynamics) which is a collaboration between Alenia, ANSYS-AEA, Chalmers University, CNRS-Lille, Dassault, DLR, EADS Military Aircraft, EUROCOPTER Germany, EDF, FOI-FFA, IMFT, Imperial College London, NLR, NTS, NUMECA, ONERA, TU Berlin, and UMIST. The project is funded by the European Community represented by the CEC, Research Directorate-General, in the 6th Framework Programme, under Contract No. AST3-CT-2003-502842.

REFERENCES

Batten, P., Goldberg, U., Chakravarthy, S., 2004. Interfacing statistical turbulence closures with large-eddy simulation. AIAA Journal 42 (3), 485–492.

Billson, M., 2004. Computational techniques for turbulence generated noise. Ph.D. thesis, Dept. of Thermo and Fluid Dynamics, Chalmers University of Technology, Göteborg, Sweden.

Billson, M., Eriksson, L.-E., Davidson, L., 2003. Jet noise prediction using stochastic turbulence modeling. AIAA paper 2003-3282, 9th AIAA/CEAS Aeroacoustics Conference.

Dahlström, S., Davidson, L., 2003. Large eddy simulation applied to a high-Reynolds flow around an airfoil close to stall. AIAA paper 2003-0776.

Davidson, L., Billson, M., 2004. Hybrid LES/RANS using synthesized turbulence for forcing at the interface. In: Neittaanmäki, P., Rossi, T., Korotov, S., Oñate, E., Périaux, J., Knörzer, D. (Eds.), ECCOMAS 2004. July 24-28, Finland.

Davidson, L., Billson, M., 2005. Hybrid LES/RANS using synthesized turbulence for forcing at the interface (submitted). International Journal of Heat and Fluid Flow.

Davidson, L., Dahlström, S., 2004. Hybrid LES-RANS: An approach to make LES applicable at high Reynolds number (keynote lecture). In: de Vahl Davis, G., Leonardi, E. (Eds.), CHT-04: Advances in Computational Heat Transfer III. April 19-24, Norway.

Davidson, L., Dahlström, S., 2005. Hybrid LES-RANS: An approach to make LES applicable at high Reynolds number. International Journal of Computational Fluid Dynamics (to appear).

Davidson, L., Peng, S.-H., 2003. Hybrid LES-RANS: A one-equation SGS model combined with a $k - \omega$ model for predicting recirculating flows. International Journal for Numerical Methods in Fluids 43, 1003–1018.

Emvin, P., 1997. The full multigrid method applied to turbulent flow in ventilated enclosures using structured and unstructured grids. Ph.D. thesis, Dept. of Thermo and Fluid Dynamics, Chalmers University of Technology, Göteborg.

Hamba, F., 2003. A hybrid RANS/LES simulation of turbulent channel flow. Theoretical and Computational Fluid Dynamics 16, 387–403.

Jarrin, N., Benhamadouche, S., Laurence, D., 2005. Inlet conditions for large-eddy simulation using a new vortex method. In: Humphrey, J., Eaton, J., Friedrich, R., Kasagi, N., Leschziner, M., Gatski, T. (Eds.), The Fourth International Symp. on Turbulence and Shear Flow Phenomena. Williamsburg, Virginia.

Le, H., Moin, P., Kim, J., 1997. Direct numerical simulation of turbulent flow over a backward-facing step. Journal of Fluid Mechanics 330, 349–374.

Smirnov, A., Shi, S., Celik, I., 2001. Random flow generation technique for large eddy simulations and particle-dynamics modeling. ASME: Journal of Fluids Engineering 123 (2), 359–371.

Temmerman, L., Hadžiadbic, M., Leschziner, M., Hanjalić, K., 2005. A hybrid two-layer URANS-LES approach for large eddy simulation at high Reynolds numbers. International Journal of Heat and Fluid Flow 26, 173–190.

Tucker, P., 2003. Differential equation based length scales to improve DES and RANS simulations. AIAA paper 2003-3968, 16th AIAA CFD Conference.

Tucker, P., Davidson, L., 2004. Zonal k-l based large eddy simulation. Computers & Fluids 33 (2), 267–287.

Welty, J., C.E.Wicks, Wilson, R., 1984. Fundamentals of Momentum, Heat, and Mass Transfer, 3rd Edition. John Wiley & Sons, New York.

Xiao, X., Edwards, J., Hassan, H., 2003. Inflow boundary conditions for LES/RANS simulations with applications to shock wave boundary layer interactions. AIAA paper 2003–0079, Reno, NV.